Quantum routing of single optical photons with a superconducting flux qubit

Keyu Xia (夏可宇),[1,2,3,*] Fedor Jelezko,[4,5] and Jason Twamley[2]

[1]*National Laboratory of Solid State Microstructures, College of Engineering and Applied Sciences, Nanjing University, Nanjing 210093, China*

[2]*ARC Centre for Engineered Quantum Systems, Department of Physics and Astronomy, Macquarie University, NSW 2109, Australia*

[3]*Theoretical Quantum Physics Laboratory, RIKEN Cluster for Pioneering Research, Wako, Saitama 351-0198, Japan*

[4]*Institute of Quantum Optics, Ulm University, 89081 Ulm, Germany*

[5]*Center for Integrated Quantum Science and Technology (IQST), Ulm University, 89081 Ulm, Germany*

(Received 23 January 2018; published 14 May 2018)

Interconnecting optical photons with superconducting circuits is a challenging problem but essential for building long-range superconducting quantum networks. We propose a hybrid quantum interface between the microwave and optical domains where the propagation of a single-photon pulse along a nanowaveguide is controlled in a coherent way by tuning the electromagnetically induced transparency window with the quantum state of a flux qubit mediated by the spin in a nanodiamond. The qubit can route a single-photon pulse using the nanodiamond into a quantum superposition of paths without the aid of an optical cavity—simplifying the setup. By preparing the flux qubit in a superposition state our cavityless scheme creates a hybrid state-path entanglement between a flying single optical photon and a static superconducting qubit.

DOI: 10.1103/PhysRevA.97.052315

I. INTRODUCTION

Quantum networks are an essential component for scalable quantum information processing and quantum communication [1,2]. A key element to build a quantum network is a quantum router [3–6], which coherently communicates between distant quantum nodes using photons. A quantum router determines the outgoing channel of the input flying photons by the quantum state of a static control qubit and this must be achieved in a coherent fashion.

Solid-state qubits like superconducting qubits (SQs) working in the microwave (mw) domain are perhaps the most promising candidates for scalable quantum computation. However, communicating between remote SQs requires the transport of optical photons. A quantum interface bridging the mw and optical domains has been proposed based on optomechanical transduction [7–12], frequency mixing in ensembles of spins [13–15], or atoms [16,17]. So far, all these works require the transfer of excitations between the mw and optical domains and usually require large magnetic coupling [7–17]. In contrast, the quantum router can be more advantageous for quantum networks [3–5], since it creates state-path entanglement between a flying photon and a static qubit. So far, quantum routers can only work in the mw domain [18–20] or the optical domain [21–28] separately. However, a key challenge for SQ-based quantum networks is to achieve the hybrid quantum routing of optical photons by qubits working in the mw domain.

Here we present a scheme to route a single-photon pulse into a quantum superposition of output paths by a magnetic field generated by a flux qubit. This magnetic field is quantum because it depends on the quantum state of the flux qubit. Our cavityless scheme also creates entanglement between the propagation paths of a flying optical photon and the states of a static superconducting qubit. The quantum entanglement is "hybrid" because the entangled two particles belong to two different domains—the microwave and the optical domains. Such entanglement has only been demonstrated recently by using cavity QED in the optical domain [29]. Our scheme is able to route the optical photons with little change in pulse shape and does not directly exchange excitation between the static and flying qubits. Our scheme is tailored for a superconducting qubit—a flux qubit in particular, and does not require the demanding integration of high-Q optical cavities. In addition, in contrast to previous works making use of off-resonant strong coupling to swap excitation, the driving in our scheme is nearly on-resonance and more efficient. Our method only requires a weak magnetic spin-flux qubit coupling larger than the decoherence rates of the ground states of the single spin and the flux qubit. More importantly, we route the single photon by tuning an electromagnetically induced transparency (EIT) window of a single spin.

II. MODEL

A. System

The main idea for our quantum routing of a single traveling photon with a flux qubit is depicted in Fig. 1. A single-photon pulse propagating in a nanowaveguide is dominantly scattered forward and backward by a Λ-type three-level "atom" like a silicon vacancy defect (SiVs) in a nanodiamond. Our scheme requires the strong optical coupling regime and such large coupling strengths in a waveguide setup can be achieved using various nanostructures [35–43]. In our proposal the atom acts as a beam splitter to control the transmission and reflection of the input single-photon pulse. An external classical laser

*keyu.xia@mq.edu.au

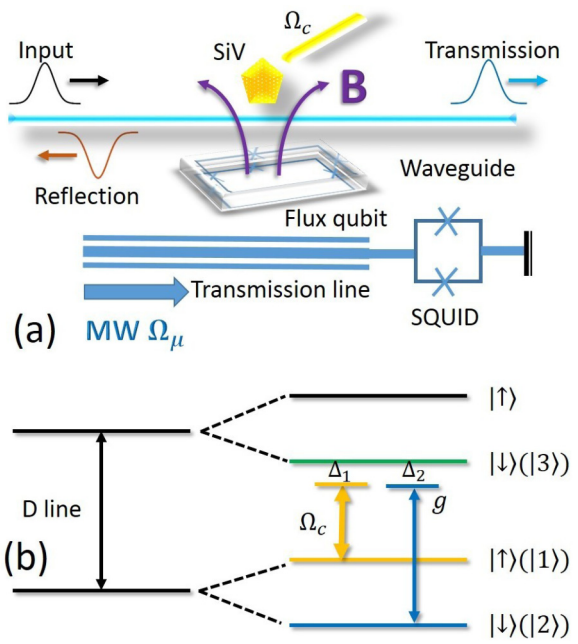

FIG. 1. (a) Schematic of a hybrid quantum single-photon router at 20mK. A single-photon pulse with carrier frequency of $\omega_{\rm in}$ (right moving pulse on top left) inputs to a nanowaveguide, e.g., a nanofiber or a photonic crystal waveguide, from the left. It couples to a nearby single SiV with strength g. An external coherent laser field Ω_c drives a transition in the SiV and creates an EIT window. It can be tuned from less than kHz to many MHz. This varying region is large enough for our scheme requiring an energy shift of a few kHz. The input pulse partly passes through the SiV (right moving pulse on top right) and is partly scattered backwards (left moving pulse—upside down on top left). The central frequency of the EIT window is modulated by the energy levels of the SiV, which themselves are shifted due to the quantum magnetic field B (outward pointing vectors surrounding the SiV) dependent on the quantum state of the flux qubit, $|e\rangle$ and $|g\rangle$. A classical microwave field, Ω_μ, from a nearby SQUID-terminated transmission line [30,31], modulates the flux qubit energies quickly in time. The SQUID is also used to isolate the flux noise in the transmission line from the flux qubit [30–32]. (b) Level diagram of the SiV. The SiV acts as a Λ-type configuration with the excited state $|3\rangle$, and two ground states $|2\rangle$ and $|1\rangle$ [33,34].

pulse, Ω_c, is applied to open an EIT window for the input single photon. It can be tuned from less than kHz to many MHz, dependent on the intensity of the laser beam. For a long input single-photon pulse nearly resonant with the transition of $|2\rangle \leftrightarrow |3\rangle$, under the condition of two-photon resonance, the atom is transparent and the single photon can remain right moving, whereas the single photon is completely reflected backward when two-photon detuning is large but the single photon is nearly resonant with the atom. Therefore, shifting the energy levels of the atom can control the transmission and reflection of the incident single photon. To do so, a magnetic field $\mathbf{B}$ created by a flux qubit with the ground and excited states $|g\rangle$ and $|e\rangle$ is applied to shift the levels of $|1\rangle$, $|2\rangle$, and $|3\rangle$. This quantum magnetic field is dependent on the quantum state of the flux qubit. As a result, one can use the flux qubit to route the input single photon to a superposition state of two output paths. Essentially, this device can create hybrid entanglement between a flying optical photon and a static superconducting qubit.

We assume that the involved three levels, $|j\rangle$, of SiV have energies ω_j with $j \in \{1,2,3\}$. The coherent laser field with frequency $\omega_{\rm c}$ and the traveling single photon with carrier frequency $\omega_{\rm in}$ drive the transitions $|1\rangle \leftrightarrow |3\rangle$ and $|2\rangle \leftrightarrow |3\rangle$ with detunings

$$\Delta_1 = (\omega_3 - \omega_1 - \omega_{\rm c}), \tag{1a}$$

$$\Delta_2 = (\omega_3 - \omega_2 - \omega_{\rm in}), \tag{1b}$$

respectively. The SiV is a spin-$\frac{1}{2}$ system. Specifically, the level $|1\rangle$ is spin up, while the levels $|2\rangle$ and $|3\rangle$ are spin down. $g_{{\rm e},j} \approx 1$ is the g factor of these spin-$\frac{1}{2}$ levels. The energies of these states can be shifted by a magnetic field due to the Zeeman effect. Here the magnetic field is generated by the flux qubit and is dependent on the quantum state of the flux qubit, i.e., $\mathbf{B}\sigma_z'$, where $\sigma_z' = |e\rangle\langle e| - |g\rangle\langle g|$. It decays at a rate of γ_f and has a pure dephasing rate Γ^*. We arrange that the diamond is cut along the z direction and $\mathbf{B}$ orients to z as well. Similar to the energy shift in a nitrogen vacancy center by a magnetic field [44], the level $|j\rangle$ of SiV shifts by an energy

$$\pm\eta_j\sigma_z' = \pm\mu_B g_{{\rm e},j}\mathbf{B}\sigma_z', \tag{2}$$

with $\eta_j = \mu_B g_{{\rm e},j}$ and $j \in \{1,2,3\}$, where $\mu_B = 14$ GHz/T, with μ_B being the Bohr magneton. In such an arrangement, the energy shifts of SiV due to the flux qubit are given by $(\eta_1 S_{11} - \eta_3 S_{33} - \eta_2 S_{22})\sigma_z'$ with $S_{lj} = |l\rangle\langle j|$ and $l, j \in \{1,2,3\}$. When the flux qubit is prepared in the state $|e\rangle$, the jth level is shifted up ($j = 1$) or down ($j = 2,3$) by η_j, whereas the shift is reversed to $-\eta_j$ for $|g\rangle$. The real two-photon detuning is

$$\delta = \Delta_1 - \Delta_2 - (2\eta_3 + \eta_1 - \eta_2)\,\langle\sigma_z'\rangle. \tag{3}$$

The reason we make use of a SiV center is that it is expected to have very long decoherence time, T_2, for the spin at mK temperatures [45].

A classical magnetic field Ω_μ is applied to prepare the initial state, and then rapidly modulates the energy levels of the flux qubit through a transmission line (TL) terminated by a superconducting quantum interference device (SQUID) [31,46]. This TL is a one-dimensional environment causing flux noise. The flux qubit dominantly decays via the magnetic coupling to this TL [47–49]. Its decay rate γ_f is determined by the coupling to the flux noise in the TL. The SQUID can also be used to control the relaxation of the flux qubit, caused by the flux noise at on-resonance frequencies. The applied microwave field and the noise propagate along the TL and are reflected at the end of the TL [right end in Fig. 1(a)]. Both the reflected and the right-moving mode couple to the flux qubit. They form a standing wave. The SQUID can be used to induce a phase difference between them. Thus the positions of antinode and node of the standing wave can be tuned by the phase shift imparted by the SQUID. During initialization, we tune the SQUID so that the antinode is at the position of the qubit. In this case, the applied mw field can quickly prepare the qubit to the desired state. After that, we switch off the coupling of the qubit to the TL by inducing a π phase shift in the reflected mode by modulating the SQUID, thus moving the node to coincide with the position of the qubit. In doing so, the relaxation of the qubit is tuned to be negligibly small. This method, to switch off the

relaxation of the qubit, has been experimentally proved valid [30–32].

We first derive the Hamiltonian governing the dynamics of the presented hybrid quantum system. The flux qubit, with the excited state $|e\rangle$ and the ground state $|g\rangle$, creates a magnetic field **B** dependent on its inner quantum state. The transition frequency of this flux qubit can be tuned with a bias flux. If the bias flux includes a weak continuous microwave field Ω_μ oscillating at frequency ω_μ [50], the Hamiltonian for the flux qubit is

$$H_{\rm flux} = \frac{\epsilon}{2}\sigma_z' + \frac{\mathscr{T}}{2}\sigma_x' + \Omega_\mu \cos(\omega_\mu t)\sigma_z', \tag{4}$$

where $\sigma_x' = |e\rangle\langle g| + |g\rangle\langle e|$ is the spin operator for spin $\frac{1}{2}$, ϵ is the energy difference between $|e\rangle$ and $|g\rangle$, and $\mathscr{T}$ is the tunnel splitting between these two states. For a flux qubit used here, $\epsilon = 2I_p(\Phi_b - 0.5\Phi_0)$ is determined by the persistent current I_p circulating along the loop of the flux qubit and the flux bias is Φ_b [47]. Φ_0 is the quantum flux. The applied microwave field quickly modulates the transition frequency of the tunable-gap flux qubit [50]. At the so-called sweet point, $\epsilon = 0$, and the flux qubit has the longest coherence time. $\mathscr{T}$ is normally a few GHz. Then, in the dressed basis of $|\Psi_\pm\rangle = (|e\rangle \pm |g\rangle)/\sqrt{2}$, and we can rotate the frame as $\sigma_z' \to \sigma_x$ and $\sigma_x' \to \sigma_z$ [47]. The Hamiltonian Eq. (4) in this rotated coordinate system becomes

$$H_{\rm flux} = \frac{\mathscr{T}}{2}\sigma_z + \Omega_\mu \cos(\omega_\mu t)\sigma_x. \tag{5}$$

Now the microwave field becomes a driving field. If one is at resonance, $\omega_\mu = \mathscr{T}$, we can further rotate the frame back to the bare basis of $\{|e\rangle,|g\rangle\}$. In this basis, $\sigma_z \to \sigma_x'$ and $\sigma_x \to \sigma_z'$ [47], and the Hamiltonian becomes

$$H_{\rm flux} = \frac{\Omega_\mu}{2}\sigma_z'. \tag{6}$$

When the mw field is very weak, Ω_μ is much smaller than the bandwidth of the input single-photon pulse. In this case, we can neglect the coherent motion of the flux qubit (setting $\Omega_\mu \to 0$), and only consider its decoherence. The flux qubit, when operating in the vicinity of the sweet point $\epsilon = 0$, can generate a quantum-state dependent magnetic field which is able to shift the levels of an ensemble of color centers in a diamond, as demonstrated by Zhu *et al.* [44]. Note that the level shifts of an ensemble of color centers in [44] are due to the Zeeman shift. The same physical mechanism can also induce the energy shift to a single SiV defect which we consider here.

The waveguide mode can be either left moving or right moving. The notations $C_{\rm R}^\dagger(x)$ and $C_{\rm L}^\dagger(x)$ indicate the creation of a right- or left-moving photon at position x. As shown in Fig. 1, the Λ-type three-level system, like the SiV, at $x = 0$ interacts with both the left- and right-moving photons at the carrier frequency $\omega_{\rm in}$. These waveguide modes drive the transition of $|3\rangle \leftrightarrow |2\rangle$ with a coupling rate of g. At the same time, the transition of $|3\rangle \leftrightarrow |1\rangle$ is driven by an extra coherent laser field Ω_c, with frequency ω_c. The excited state $|3\rangle$ of SiV decays to the ground state $|1\rangle$ ($|2\rangle$), with a rate of γ_1 (γ_2), while the decay, Γ, from $|1\rangle$ to $|2\rangle$ is negligibly small. Based on the above description, the Hamiltonian describing the dynamics of the whole system is given by

$$\begin{aligned} H =& [\omega_3 - i(\gamma_1+\gamma_2)]S_{33} + \omega_2 S_{22} + (\omega_1 - i\Gamma)S_{11} \\ &+ (\eta_1 S_{11} - \eta_3 S_{33} - \eta_2 S_{22})\sigma_z' \\ &+ \Omega_c\left(e^{-i\omega_c t}S_{31} + e^{i\omega_c t}S_{13}\right) \\ &+ \int dx\, C_R^\dagger(x)\left(\omega_{\rm in} - i v_g\frac{\partial}{\partial x}\right)C_R(x) \\ &+ \int dx\, C_L^\dagger(x)\left(\omega_{\rm in} + i v_g\frac{\partial}{\partial x}\right)C_L(x) \\ &+ g\int dx\,\delta(x)[(C_R^\dagger(x) + C_L^\dagger(x))S_{23} + {\rm H.c.}], \end{aligned} \tag{7}$$

where v_g is the velocity of the light in the nanowaveguide. When the flux qubit is in state $|e\rangle$ ($|g\rangle$), we have $\langle\sigma_z'\rangle = 1\,(-1)$. If we are interested in these two special states, then we can replace σ_z' with 1 or -1 in Eq. (7). Taking $|e\rangle$ for an example, under the unitary transformation

$$\begin{aligned} U_e = \exp\Big\{ & -i[(\omega_2 - \eta_2)S_{22} + (\omega_2 - \eta_2 + \omega_{\rm in})S_{33} \\ & + (\omega_2 - \eta_2 + \omega_{\rm in} - \omega_c)S_{11}]t \\ & - i\int dx\,\omega_{\rm in}(C_R^\dagger C_R + C_L^\dagger C_L)t\Big\}, \end{aligned} \tag{8}$$

the Hamiltonian of Eq. (7), in the rotating frame can be written as

$$\begin{aligned} H_e =& [(\Delta_2 + \eta_2 - \eta_3) - i(\gamma_1+\gamma_2)]S_{33} \\ &+ [(\Delta_2 - \Delta_1 + \eta_1 + \eta_2) - i\Gamma]S_{11} + \Omega_c(S_{31} + S_{13}) \\ &- i v_g\int dx\, C_{\rm R}^\dagger(x)\frac{\partial}{\partial x}C_{\rm R} + i v_g\int dx\, C_{\rm L}^\dagger(x)\frac{\partial}{\partial x}C_{\rm L} \\ &+ g\int dx\,\delta(x)[(C_{\rm R}^\dagger + C_{\rm L}^\dagger)S_{23} + (C_{\rm R} + C_{\rm L})S_{32}]. \end{aligned} \tag{9}$$

Here the single-photon detunings are

$$\Delta_1 = (\omega_3 - \omega_1) - \omega_c, \tag{10a}$$

$$\Delta_2 = (\omega_3 - \omega_2) - \omega_{\rm in}. \tag{10b}$$

For the flux qubit in state $|g\rangle$, η_j changes to $-\eta_j$. Combining these two cases gives the Hamiltonian describing the interaction between the propagating photon and the "static" subsystem as

$$\begin{aligned} H^{(1)} =& [(\Delta_2 \pm \eta_2 \mp \eta_3) - i(\gamma_1+\gamma_2)]S_{33} \\ &+ (\Delta_2 - \Delta_1 \pm \eta_1 \pm \eta_2)S_{11} + \Omega_c(S_{31} + S_{13}) \\ &- i v_g\int dx\, C_{\rm R}^\dagger(x)\frac{\partial}{\partial x}C_{\rm R} + i v_g\int dx\, C_{\rm L}^\dagger(x)\frac{\partial}{\partial x}C_{\rm L} \\ &+ g\int dx\,\delta(x)[(C_{\rm R}^\dagger + C_{\rm L}^\dagger)S_{23} + (C_{\rm R} + C_{\rm L})S_{32}]. \end{aligned} \tag{11}$$

The upper (lower) sign in front of η_j in Eq. (11) corresponds to the flux qubit state $|e\rangle$ ($|g\rangle$). The overall dephasing of the SiV center and the flux qubit limit the usable η_j, and subsequently the required amplitude of the magnetic field generated by the flux qubit. The decay of state $|1\rangle$ of SiV is negligible at 20mK. The right- and left-moving wave packets of photons can be

written as

$$|\Phi_R\rangle = \tilde{\phi}_R(x)C_{\rm R}^\dagger(x)|\varnothing\rangle, \tag{12a}$$

$$|\Phi_L\rangle = \tilde{\phi}_L(x)C_{\rm L}^\dagger(x)|\varnothing\rangle, \tag{12b}$$

where $|\varnothing\rangle$ is the vacuum state of the waveguide mode. The corresponding excitations in the right- and left-moving modes are given by

$$e_R = \int dx\, |\tilde{\phi}_R(x)|^2, \tag{13a}$$

$$e_L = \int dx\, |\tilde{\phi}_L(x)|^2. \tag{13b}$$

We define a contrast measure for routing as $\mathfrak{C} = |e_R - e_L|/(e_R + e_L)$. Note that Fan's method can only treat the flux qubit either in $|e\rangle$ or $|g\rangle$ separately [51,52].

B. Steady-state solution

In this section we will find the steady-state transmission and reflection of the input single photon by using a method developed by Fan *et al.* [51,52]. In Fan's method, the general state can be expressed as

$$|\Phi(t)\rangle = \left[\int dx\, \tilde{\phi}_R(x)C_{\rm R}^\dagger(x) + \tilde{\phi}_L(x)C_{\rm L}^\dagger(x)\right]|\varnothing,2\rangle \otimes (\alpha|g\rangle + \beta|e\rangle) + [\tilde{e}_3|\varnothing,3\rangle + \tilde{e}_1|\varnothing,1\rangle] \otimes (\alpha|g\rangle + \beta|e\rangle),$$

where $\tilde{\phi}_{R/L}(x,t)$, is the single-photon wave function in the right- or left-moving modes and $\tilde{e}_1$ and $\tilde{e}_3$ are the excitation amplitudes of the SiV in state $|1\rangle$ and $|3\rangle$, respectively. For this general state, the Schrödinger's equation $i\frac{\partial|\Phi(t)\rangle}{\partial t} = H^{((1))}|\Phi(t)\rangle$ gives the following set of equations of motion:

$$i\frac{\partial}{\partial t}\tilde{e}_1 = (\Delta_2 - \Delta_1 \pm \eta_1 \pm \eta_2 - i\Gamma)\tilde{e}_1 + \Omega_c\tilde{e}_3, \tag{14a}$$

$$i\frac{\partial}{\partial t}\tilde{e}_3 = \left[(\Delta_2 \pm \eta_2 \mp \eta_3) - i(\gamma_1+\gamma_2)\right]\tilde{e}_3 + \Omega_c\tilde{e}_1 + [\tilde{\phi}_R(0,t) + \tilde{\phi}_L(0,t)]g, \tag{14b, 14c}$$

$$i\frac{\partial}{\partial t}\tilde{\phi}_R(x,t) = -iv_g\frac{\partial}{\partial x}\tilde{\phi}_R(x,t) + g\tilde{e}_3, \tag{14d}$$

$$i\frac{\partial}{\partial t}\tilde{\phi}_L(x,t) = iv_g\frac{\partial}{\partial x}\tilde{\phi}_L(x,t) + g\tilde{e}_3. \tag{14e}$$

Here we set $\hbar = 1$. To solve the steady-state transmission and reflection, we define the untilded symbols for the slowly varying envelopes of the wave functions and the excitation amplitudes so that $\tilde{X} = e^{-i(\omega-\omega_{\rm in})t}X$, with $X \in \{\phi_R,\phi_L,e_3,e_1\}$. Our aim is to solve for the steady-state transmission and reflection for an incident photon. For this purpose, we take

$$\phi_R(x) = e^{iQx}[\theta(-x) + t\theta(x)], \tag{15a}$$

$$\phi_L(x) = r\,e^{-iQx}\theta(-x), \tag{15b}$$

where $Q = (\omega - \omega_{\rm in})/v_g$, t is the transmission amplitude, and r is the reflection amplitude [51,52]. $\theta(x)$ is the Heaviside step function and has the relations

$$\theta(x)|_{x=0} = 1/2, \tag{16a}$$

$$\frac{\partial\theta(x)}{\partial x}|_{x\to 0_+} = 1, \tag{16b}$$

$$\frac{\partial\theta(-x)}{\partial x}|_{x\to 0_-} = -1. \tag{16c}$$

We define the even mode as

$$\phi_e(x) = [\phi_R(x) + \phi_L(-x)]/\sqrt{2} = \frac{1}{\sqrt{2}}e^{iQx}[\theta(-x) + t_e\theta(x)], \tag{17}$$

yielding $t_e = t + r$. We set $\dot{X} = 0$ for the steady state. We can find the amplitudes of transmission and reflection for a single-photon input as

$$t = (t_{\rm e} + 1)/2, \tag{18a}$$

$$r = (t_{\rm e} - 1)/2, \tag{18b}$$

with $t_{\rm e} = \frac{[(\Delta_2-\Delta_1)\pm\eta_1\pm\eta_2][\Delta_2\pm\eta_2\mp\eta_3+i\Gamma_{\rm wg}-i(\gamma_1+\gamma_2)]-\Omega_c^2}{[(\Delta_2-\Delta_1)\pm\eta_1\pm\eta_2][\Delta_2\pm\eta_2\mp\eta_3-i\Gamma_{\rm wg}-i(\gamma_1+\gamma_2)]-\Omega_c^2}$. Here, $\Gamma_{\rm wg} = g^2/v_g$ is the rate of the SiV to emit photons into the nanowaveguide [51,52]. The transmission and reflection are $T = |t|^2$ and $R = |r|^2$, respectively, and these quantities represent the probabilities for the excitations of right- and left-moving scattered wave packets for a right-moving single-photon input. The derived analytic formula can guide us to find the working window for routing a single photon. For simplicity, we assume that $\eta_1 = \eta_2 = \eta_3 = \eta$ for all investigation below.

C. Cascaded open system description

Fan's scheme is very powerful for studying the dynamics of a system interacting with traveling photons but is hard to take into account the decoherence of the system. Instead we consider a cascaded master equation with a source cavity injecting a photon into the nanowaveguide-SiV quantum system while also including the dephasing of the system [53,54]. This method eliminates the explicit waveguide mode in the Hamiltonian and is widely used to study quantum systems with nonclassical inputs [11,12,15]. The cascaded master equation method also can be used to evaluate the entanglement and the fidelity of the scattered state, where the latter measures how close the scattered state is to a particular target state. We use a "source" cavity to provide a single-photon pulse. This source is equivalent to the single-photon wave packet in Fan's scheme after applying the relation $x = v_g t$. By assuming a time-dependent decay rate of the source cavity we can generate an arbitrary wave function for the single-photon wave packet incoming to the nanowaveguide-SiV system. The single photon from the source cavity directly drives the transition of $|2\rangle \leftrightarrow |3\rangle$ after a delay, which can be assumed to be zero. Following [53,54], the dynamics of our system can be described by the Hamiltonian

$$H^{(2)}/\hbar = H_{\rm R} + H_{\rm SiV} + H_{\rm flux} + H_{\rm I}, \tag{19}$$

with

$$H_{\rm R} = \omega_{\rm in} a^\dagger a, \tag{20a}$$

$$H_{\rm flux} = \frac{\Omega_\mu}{2}\sigma_z', \tag{20b}$$

$$H_{\rm SiV} = \sum_j \omega_j S_{jj} + \Omega_c(e^{-i\omega_c t}S_{31} + e^{i\omega_c t}S_{13}), \tag{20c}$$

$$H_{\rm I} = (\eta_1 S_{11} - \eta_2 S_{22} - \eta_3 S_{33})\sigma_z', \tag{20d}$$

and a superoperator linking the cavity and the atom is

$$\mathscr{L}_{\rm Net}\rho = -\sqrt{\xi_c\kappa_c\xi_2\Gamma_2}(S_{32}a\rho - a\rho S_{32} + \rho a^\dagger S_{23} - S_{23}\rho a^\dagger), \tag{21}$$

with

$$\xi_c = \frac{\kappa_{\rm ex}}{\kappa_c} \leqslant 1, \tag{22a}$$

$$\xi_2 = \frac{\Gamma_{\rm wg}}{\Gamma_2} \leqslant 1/2. \tag{22b}$$

κ_c is the total decay rate of the source cavity and $\Gamma_2 = \gamma_2 + 2\Gamma_{\rm wg}$ is the total decay from $|3\rangle$ to $|2\rangle$. $\kappa_{\rm ex}$ and $\Gamma_{\rm wg}$ are the decay into the waveguide from the source cavity and the SiV, respectively. Note that the SiV decays into two channels: the right- and left-moving modes with the rate $\Gamma_{\rm wg}$ for each. The parameters, $\xi_c = 1$ and $\xi_2 = 0.5$, indicate all excitation decays into the nanowaveguide from the source cavity and the SiV center, respectively. $H_{\rm R}$ is the cavity model used to generate an arbitrary single-photon pulse in cascade. To create a single-photon input pulse in the nanowaveguide we can set this source cavity initially in the Fock state $|1\rangle$. The wave function of the input single photon can be controlled by a time-dependent decay from this source cavity $\kappa_c(t)$, and we assume $\kappa_c(t) = 2\Gamma_{\rm wg}e^{-(t-\tau)^2/2\tau_p^2}$ with a duration of τ_p and a delay $\tau = 5.5\tau_p$ to provide a Gaussian-like single-photon pulse. Such delay is large enough to ensure the waveguide is initially in the vacuum state. $H_{\rm SiV}$ describes the free Hamiltonian and the classical driving of the SiV. $H_{\rm flux}$ is the Hamiltonian describing the evolution of the flux qubit modulated by the classical mw field. The energy shifts of the SiV states due to the flux qubit are given by $H_{\rm I}$.

To eliminate the fast rotating terms in Eq. (19), we apply the unitary transformation

$$U_2 = \exp\left\{-i\left[\omega_{\rm in}a^\dagger a + \frac{\Omega_\mu}{2}\sigma_z'\right]t\right\} \otimes \exp\{-i[\omega_3 S_{33} + (\omega_3 - \omega_{\rm in})S_{22} + (\omega_3 - \omega_c)S_{11}]t\}, \tag{23}$$

and rewrite the Hamiltonian in Eq. (19) as

$$H^{(2)} = -\Delta_2 S_{22} - \Delta_1 S_{11} + \Omega_c(S_{31} + S_{13}) + H_{\rm I}. \tag{24}$$

The dynamics of the system can be completely described by the master equation

$$\dot\rho = -i[H^{(2)},\rho] + \mathscr{L}_{\rm Net}\rho + \mathscr{L}(\kappa_c,a)\rho + \mathscr{L}(\gamma_1,\sigma_{13})\rho + \mathscr{L}(\Gamma_2,\sigma_{23})\rho + \mathscr{L}(\gamma_f,\sigma_{ge})\rho + \mathscr{L}(\Gamma^*,\sigma_{ee}-\sigma_{gg})\rho, \tag{25}$$

where $\mathscr{L}(\gamma,A)\rho = \gamma/2\{2A\rho A^\dagger - A^\dagger A\rho - \rho A^\dagger A\}$ with $\sigma_{ge} = |g\rangle\langle e|$ and $\sigma_{eg} = \sigma_{ge}^\dagger$. γ_f and Γ^* are the decay and pure dephasing rate of the flux qubit, respectively. The SiV interacts with both the right- and left-moving photons. Therefore, the transmitted (right-moving) and reflected (left-moving) photons can be determined according to the input-output relation [53,54] as

$$C_R(x) = \sqrt{\xi_c\kappa_c(t)}\,a(t) + \sqrt{\xi_2\Gamma_2}\,\sigma_{32}(t), \tag{26a}$$

$$C_L(x) = \sqrt{\xi_2\Gamma_2}\,\sigma_{32}(t). \tag{26b}$$

Here we use the fact that $x = v_g t$ and set $v_g = 1$.

The main goal of our scheme is to create an entangled state between the flying photon and the static superconducting qubit. In the basis of $\{C_{\rm R}^\dagger(x)|\varnothing,g\rangle, C_{\rm R}^\dagger(x)|\varnothing,e\rangle, C_{\rm L}^\dagger(x)|\varnothing,g\rangle$, and $C_{\rm L}^\dagger(x)|\varnothing,e\rangle\}$, we consider the initial state of the input photon as a right-moving single photon, $C_R^\dagger(x)|\varnothing,g\rangle$, and the flux qubit to be in the state $|\Psi_{\rm f,in}\rangle = (\alpha|g\rangle + \beta|e\rangle)$ with $|\alpha|^2 + |\beta|^2 = 1$. Without loss of generality we can assume that α is a positive real number, and $\beta = |\beta|e^{i\theta}$. We aim to create a target entangled state where the photon is conditionally reflected if the flux qubit is in the excited state

$$|\Phi_T(x,t\to\infty)\rangle = \overline{\phi}_R(x)e^{i\Theta(x)/2}C_{\rm R}^\dagger(x)|\varnothing,g\rangle - \overline{\phi}_L(x)e^{-i\Theta(x)/2}e^{i\varphi}C_{\rm L}^\dagger(x)|\varnothing,e\rangle, \tag{27}$$

where $\Theta(x)$ is a spatial phase factor due to the opposite propagation directions of the two parts of the propagating wave functions. We note that the phase Θ does not appear when taking the absolute value of the spatial overlap between the wave packet components defined as

$$|1_R\rangle =: \bar{\bar{\phi}}_R(x)C_{\rm R}^\dagger(x)|\varnothing\rangle, \tag{28a}$$

$$|1_L\rangle =: \bar{\bar{\phi}}_L(x)C_{\rm L}^\dagger(x)|\varnothing\rangle, \tag{28b}$$

which are a measure of the coherence. Here, φ is a trivial small phase offset. We choose $\int|\bar{\bar{\phi}}_R(x)|^2dx = 1$ and $\int|\bar{\bar{\phi}}_L(x)|^2dx = 1$. We have that $|1_R\rangle$ denotes a single photon in the right-moving mode over the whole waveguide, while $|1_L\rangle$ describes a left-moving single photon. Ideally, we have

$$\int|\bar\phi_R(x)|^2dx = |\alpha|^2, \tag{29a}$$

$$\int|\bar\phi_L(x)|^2dx = |\beta|^2, \tag{29b}$$

yielding $\bar\phi_R(x) = \alpha\bar{\bar\phi}_R(x)$ and $\bar\phi_L(x) = \beta\bar{\bar\phi}_L(x)$. We define the overlap fidelity with a target state as

$$F(\varphi) = \int dx\,{\rm Tr}[\rho|\Phi_T(x)\rangle\langle\Phi_T(x)|] = |\alpha|^2\int dt\,{\rm Tr}[\rho(t)C_{\rm R}^\dagger|\varnothing,g\rangle\langle\varnothing,g|C_{\rm R}] + |\beta|^2\int dt\,{\rm Tr}[\rho(t)C_{\rm L}^\dagger|\varnothing,e\rangle\langle\varnothing,e|C_{\rm L}]$$

$$+\alpha\beta^* \int dt\, e^{i\Theta(t)+i\varphi}\mathrm{Tr}[\rho(t)C_R^\dagger|\varnothing,g\rangle\langle\varnothing,e|C_L]$$
$$+\alpha^*\beta \int dt\, e^{-i\Theta(t)-i\varphi}\mathrm{Tr}[\rho(t)C_L^\dagger|\varnothing,e\rangle\langle\varnothing,g|C_R]. \quad (30)$$

The coherence at the position x is given by

$$\mathscr{C}(x) = -e^{i\Theta(x)+i\varphi}\mathrm{Tr}[\rho C_R^\dagger|\varnothing,g\rangle\langle\varnothing,e|C_L]. \quad (31)$$

This definition removes the fast oscillating phase between the two opposite propagating paths. The total coherence for the whole hybrid entangled state is evaluated as

$$\mathscr{C}_{\mathrm{sys}} = \int dx\, \mathscr{C}(x). \quad (32)$$

To show the entanglement between the output photon and the flux qubit, we also calculate the concurrence, C, in the basis of $\{|1_R,g\rangle,|1_R,e\rangle,|1_L,g\rangle,|1_L,e\rangle\}$. We first calculate the reduced density matrix of the moving photon and the static flux qubit as

$$\rho_{\text{ph-flux}}(t) = \sum_{A,B,l,k} \mathrm{Tr}\{\rho(t)C_A^\dagger|l\rangle\langle k|C_B\}|1_A,l\rangle\langle k,1_B|, \quad (33)$$

with $A,B \in \{R,L\}$ and $l,k \in \{e,g\}$, by partial tracing over the SiV. Once this reduced density matrix is known in this basis we can calculate the concurrence between the moving wave packets using the method developed by Wootters [55] as follows: (i) we first find the time-dependent spin-flipped density matrix by

$$\tilde{\rho}_{\text{ph-flux}}(t) = (M\otimes M)\rho^*_{\text{ph-flux}}(t)(M\otimes M), \quad (34)$$

where $\rho^*_{\text{ph-flux}}(t)$ is the complex conjugate of $\rho_{\text{ph-flux}}(t)$, and the matrix

$$M = \begin{pmatrix} 0 & -i \\ i & 0 \end{pmatrix}$$

denotes the standard time reversal operation on a spin-$\frac{1}{2}$ particle. (ii) We then calculate the time-dependent Hermitian matrix

$$R(t) = \sqrt{\sqrt{\rho_{\text{ph-flux}}(t)}\tilde{\rho}_{\text{ph-flux}}(t)\sqrt{\rho_{\text{ph-flux}}(t)}}, \quad (35)$$

(iii) then solve for the eigenvalues λ_j ($j \in \{1,2,3,4\}$), in decreasing order, of the Hermitian matrix $R(t)$ at t. (iv) We can calculate the concurrence density at x by

$$C(x) = \max\{0,\lambda_1(x) - \lambda_2(x) - \lambda_3(x) - \lambda_4(x)\}. \quad (36)$$

Here we use the fact that $x = v_g t$ and set $v_g = 1$ again. (v) Finally the total concurrence for the whole wave packets is evaluated as the integral of concurrence density, i.e., $C = \int dx\, C(x)$. We simply write the above calculation for the concurrence as

$$C = \int C[\rho_{\text{ph-flux}}(t)]dt. \quad (37)$$

The method developed by Fan *et al.* can easily derive the analytic form of the steady-state solution of the system without any decoherence effects arising from relaxation and pure dephasing. In contrast, the master equation model can provide a full numerical solution of the system taking into account decoherence. The master equation method can completely recover the steady-state transmission and reflection derived from Fan's method by using a long enough input pulse. These two methods yield equivalent steady-state solutions for a single-photon input if the decoherence is negligible. The analytic formula can be useful for finding a working window.

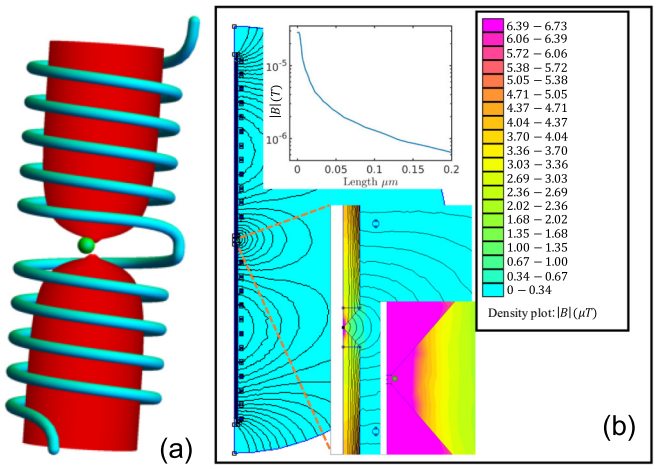

FIG. 2. Estimation of the magnetic field at the location of the SiV generated by the flux qubit. (a) Schematic of the coiled part of flux qubit to enhance the magnetic field at the SiV location. The flux qubit has a 24-turn coiled edge (helical tube). A μ-metal bowtie flux concentrator (tapered cylinder), with a relative permeability of $\mu_r = 10^6$, is inserted inside the coil to greatly enhance the local magnetic field generated by the flux qubit. The SiV (central sphere) is located near to the tip of the concentrator. The surface of the helical coil is about 240 nm away from the μ metal to avoid any flux noise caused by the flux concentrator. (b) The distribution of magnetic field around the structure in (a) is numerically solved in two-dimensional space with the free software FEMM4.2. The density plot inset shows the zoomed-in distribution close to the concentrator tips, while the line plot inset shows the distribution along the middle line joining the two tips. The small green ball in the inset indicates the position of the SiV.

D. Available coupling strength

Before demonstrating the quantum routing of single optical photons using our setup we numerically estimate the magnetic field generated by the flux qubit at the location of the SiV using the 4.2 version of the free software FEMM. We engineer a sophisticated design that can enhance this coupling. This simulation is important as it can give an indication of the maximal strength of the qubit-SiV coupling. Figure 2(a) depicts the structure for enhancing the magnetic field with a μ-metal bowtie-shaped flux concentrator. One edge of the flux qubit is a 24-turn coil with a bowtie flux concentrator inside. We assume that the wire of flux qubit has a radius of 50 nm and the persistent current leading along the flux qubit is 500 nA. The gap between two turns is 1 μm. The flux concentrator can be made from μ metal such as yttrium iron garnet (YIG) [56] with a relative permeability of $\mu = 10^6$ [57]. Such bowtie

structure has been demonstrated to be capable of focusing a magnetic field efficiently [58]. The larger end of the bowtie is a cylinder with radius of 260 nm. The tips of the bowtie end have an end radius of 5 nm. The gap between two tips is 5 nm. Although the tip of the bowtie-structured flux concentrator in [58] is much larger than that required in our scheme, nanosized ferromagnetic materials possessing a giant magnetic field have been made for disk drive write heads [59]. Moreover, a nanomagnetostructure has been practically proposed for amplification of weak magnetic field [60]. The distance from the surface of the μ metal to the coil of the flux qubit is 240 nm, which is far enough away to isolate the qubit from the flux noise introduced by the μ-metal material. As shown in Fig. 2(b) and the inset, the magnetic field located a distance 5 nm away from the center of the bowtie can be $\sim$21 μT, yielding a coupling strength $\eta/2\pi \sim 300$ kHz. This coupling is strong enough for our single-photon router. The closest turn of the coil is a few μm away from the SiV. Our design has an advantage over an alternative state-of-the-art design that uses a 15 nm spatial separation of the NV to a nearby superconducting nanowire [61]. Our design pushes the SiV spatially away from the superconducting components so as to avoid any loss of superconductivity of the flux qubit due to the optical fields illuminating the SiV. We assume that the nanowaveguide is a short plasmonic transmission line [42], so that the SiV and the nanowire can be inserted into the free space of the bowtie tip. Therefore, the fabrication of the proposed nanosize flux concentrator is feasible using the existing experimental technology.

Note that the coil nanostructure around the μ metal may introduce an external inductance $L_{\rm coil}$ to the flux qubit. Here, we provide a rough estimation of this inductance. It can be seen from Fig. 2(b) that the magnetic field in the μ metal quickly and exponentially decays to about 2 μT at 0.2 μm away from the tip, then gradually increases to $\sim$2.7 μT. The cross-sectional area of the coil is 21 μm^2 with small air gap between the coil and the surface of the μ metal, yielding a flux through the coil less than $2.8\times10^{-4}\Phi_0$, where Φ_0 is the magnetic flux quantum. Using a persistent current of size $I = 500$ nA, we obtain an inductance of $L_{\rm coil} \sim 1$ nH, which is comparable to the inductance of a Josephson junction with a critical current $I_c \approx 287$ nA. Since the inductance of the coil is therefore smaller than that of a flux qubit with a persistent current of $I_p = 500$ nA, the coil's inductance will have a minor effect on the flux qubit.

III. RESULTS

A. Working window

Now we determine the dependence of the transmission and reflection of a single-photon pulse upon the quantum state of the flux qubit. To show the main idea we first neglect the decay and the decoherence of the system by setting $\gamma_f = 0$, $\Gamma^* = 0$. Choosing appropriate parameters we can find a working EIT window for a small $\eta = 10^{-3}\Gamma_{\rm wg}$; see Fig. 3. From this we observe that the quantum state of the flux qubit can modulate the propagation of a single-photon pulse quite well around $|\Delta_2| = 2|\eta|$, with a bandwidth of $\Delta\omega = 2\Omega_c^2/\Gamma_{\rm wg}$, if the EIT window is narrow, e.g., $\Omega_c = 0.03\Gamma_{\rm wg}$.

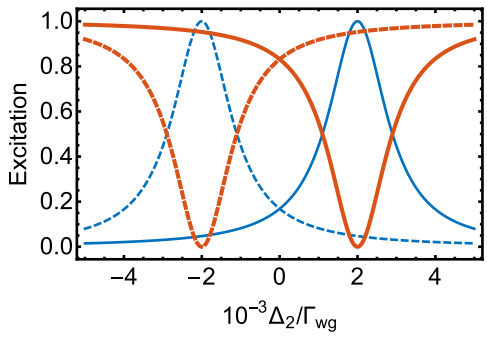

FIG. 3. Steady-state transmission (blue lines with a maximum at an abscissa of ±2) and reflection (red lines with a minimum at an abscissa of ±2) given by Eq. (18) for the excited state (dashed lines) and ground state (solid lines) of the flux qubit. We set $\Omega_c/\Gamma_{\rm wg} = 0.03$, $\eta/\Gamma_{\rm wg} = 10^{-3}$, $\Delta_1 = 0$, $\gamma_f = 0$, $\Gamma^* = 0$, $\xi_c = 1$, and $\xi_2 = 0.5$.

B. Routing and path entanglement

We now investigate the dynamics of the right- and left-moving wave packets for an input single-photon pulse; see Fig. 4. The excitation of the source cavity first decays slowly and then quickly decays to zero. As a result, the input pulse contains a single excitation, and is of finite duration $\tau_p\Gamma_{\rm wg} = 10^4$, which is within the bandwidth of the right-hand working

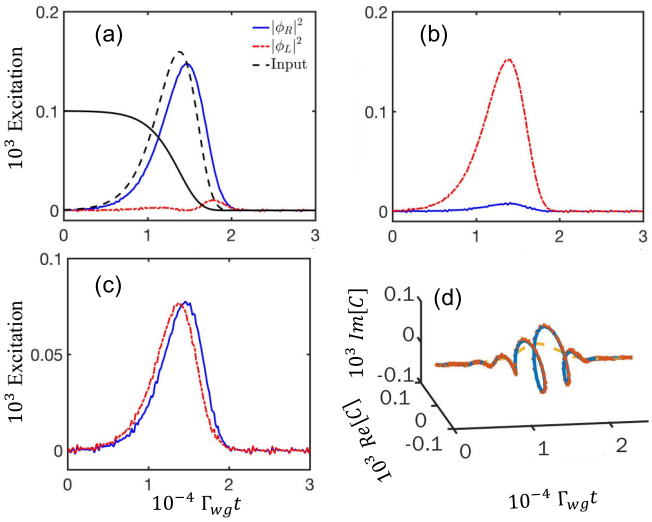

FIG. 4. (a)–(c) Time evolution of excitations of right (blue lines) and left (red lines) -moving photons with the initial state of the flux qubit (a) in $|g\rangle$, (b) in $|e\rangle$, and (c) in $(|g\rangle + |e\rangle)/\sqrt{2}$. (d) The coherence for the flux qubit prepared in $(|g\rangle + |e\rangle)/\sqrt{2}$. The blue solid line shows $\mathrm{Tr}[\rho C_{\rm R}^\dagger|\varnothing,g\rangle\langle\varnothing,e|C_{\rm L}]$ indicating the coherence density modulated by the fast spatial (time) oscillating phase $\Theta(x)$. It is fitted by $-|\bar{\phi}_R(x)||\bar{\phi}_L(x)|e^{i(\eta_1+\eta_3)x+i\varphi+i\theta}$ (the purple line). The yellow line is for the real coherence evaluated by $\mathscr{C}(x)$. In (a), the dashed black line shows the input pulse and the solid black line is for the time-dependent excitation in the source cavity. Other parameters are $\Omega_c/\Gamma_{\rm wg} = 0.03$, $\eta/\Gamma_{\rm wg} = 10^{-3}$, $\Delta_1 = 0$, $\Delta_2 = 2\eta$, $\gamma_f = 0$, $\Gamma^* = 0$, $\xi_c = 1$, $\xi_2 = 0.5$, and $\tau_p\Gamma_{\rm wg} = 10^4$. $\Gamma_{\rm wg}/2\pi \approx 300$ MHz for SiV.

window in Fig. 3. When the flux qubit is prepared in $|g\rangle$, which corresponds to $\delta = 0$, see Fig. 4(a), the input pulse mostly passes through the SiV, $e_R \simeq 0.95$, and the reflection is very small, $e_L \simeq 0.05$, yielding a contrast of $\mathfrak{C} = 0.91$. When the qubit is prepared in the state $|e\rangle$, we have $\delta = -4\eta$, see Fig. 4(b), and the single-photon pulse is mostly reflected backward, and the transmission is vanishing small. In this case, we have $e_R \simeq 0.05$, and $e_L \simeq 0.95$, and obtain a contrast of $\mathfrak{C} = 0.91$. More interestingly, the input single photon is routed into a path-entangled state of right- and left-moving wave packets with $e_R \simeq e_L \simeq 0.5$, see Fig. 4(c), if the flux qubit is in the superposition state $(|g\rangle + |e\rangle)/\sqrt{2}$. In the absence of any decoherence of the flux qubit, we create an entangled state of $|1_R,g\rangle$ and $|1_L,e\rangle$, within the bipartite system of the flying photon and the static flux qubit. The fidelity is about $F(0.07\pi) = 0.943$ and the concurrence is $C = 0.92$. The coherence between $|1_R,g\rangle$ and $|1_L,e\rangle$ is shown in Fig. 4(d), and is evaluated as $\mathscr{C}_1(x) = \mathrm{Tr}[\rho C_{\mathrm{R}}^{\dagger}|\varnothing,g\rangle\langle\varnothing,e|C_{\mathrm{L}}]$. Its behavior indicates that the coherence density between $C_{\mathrm{R}}^{\dagger}|\varnothing,g\rangle$ and $C_{\mathrm{L}}|\varnothing,e\rangle$ is modulated by a fast oscillating phase $\Theta(x)$, due to the spatial phases of the opposite propagating wave functions. As a result, it describes a spiral line (see the blue line) in Fig. 4(d). Our numerical simulation shows that $\Theta(x) = (\eta_1 + \eta_3)x$ and $\varphi = 0.07\pi$ in $|\Phi_T\rangle$. Based on this finding, we fit $\mathscr{C}_1(x)$ with $-|\overline{\phi}_R(x)||\overline{\phi}_L(x)|e^{i(\eta_1+\eta_3)x+i\varphi+i\theta}$ (see the purple line). The real coherence $\mathscr{C}(x)$, where the fast spatial oscillating phase is removed, is positive, real, and resembles $|\overline{\phi}_R(x)\overline{\phi}_L(x)|$ (see the yellow line). The total coherence is $\mathscr{C}_{\mathrm{sys}} \approx 0.466$. Obviously, the transmitted and reflected pulses resemble the input pulse in all cases. If the flux qubit is prepared in the mixed state, $(|e\rangle\langle e| + |g\rangle\langle g|)/2$, the transmission and reflection is the same as in the case of a superposition state of $(|g\rangle + |e\rangle)/\sqrt{2}$, but the coherence between the photons vanishes. In the mixed case, the routing of the single photon becomes completely random.

The entangled state $|\Phi_T(x)\rangle = \alpha|1_R,g\rangle - \beta|1_L,e\rangle$ is the most interesting result of this work. It is fragile to decay and decoherence. The decay rate of the flux qubit can be reduced to be very small by decoupling it from the TL by modulating the terminating SQUID. However, the qubit's pure dephasing, Γ^*, will not reduce even when decoupled from the TL. Now we study the effects on the routing depending on the flux qubit pure dephasing (see Fig. 5). As the pure dephasing increases, the fidelity of the output state with the ideal target entangled state exponentially decreases to be that displayed by a completely mixed state, $F = 0.5$. Similarly, the concurrence also exponentially decays to zero and the entanglement disappears. In contrast, the right- and left-moving photon excitation probabilities are equal to 0.5 and are independent of the degree of pure dephasing. Thus, for large dephasing, the system classically and randomly routes the single photon into a mixture of right- and left-moving modes.

Quantum entanglement is at the heart of quantum information. The realization of entanglement between a static superconducting qubit and a flying photonic qubit is particularly desired for building quantum networks [10,62]. Furthermore, routing singe photons in a quantum way is also useful for quantum information processing [6,27].

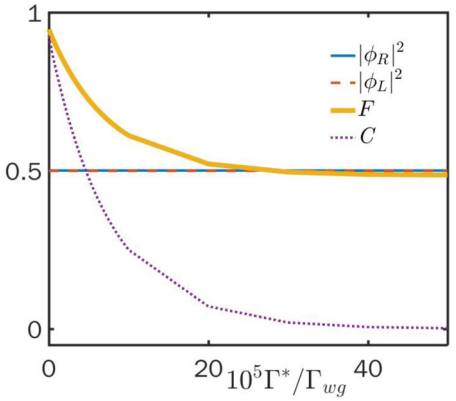

FIG. 5. Excitations ($|\phi_R|^2$, $|\phi_L|^2$), fidelity, F, and concurrence, C, as a function of the pure dephasing rate Γ^*. Other parameters are $\Omega_c/\Gamma_{\mathrm{wg}} = 0.03$, $\eta/\Gamma_{\mathrm{wg}} = 10^{-3}$, $\Delta_1 = 0$, $\Delta_2 = 2\eta$, $\gamma_f = 0$, $\xi_c = 1$, $\xi_2 = 0.5$, and $\tau_p\Gamma_{\mathrm{wg}} = 10^4$. The blue line ($|\phi_R|^2$) overlaps with that for $|\phi_L|^2$. $\Gamma_{\mathrm{wg}}/2\pi \approx 300$ MHz for SiV.

C. Heralded quantum state transfer

Next we show how to transfer a quantum state between the "flying" photonic qubit and the static flux qubit with the help of a quantum measurement. As discussed above, for a right-moving single photon and the flux qubit prepared initially in the state of $|\Psi_{\mathrm{f,in}}\rangle = (\alpha|g\rangle + \beta|e\rangle)$, our hybrid quantum system can generate an entangled state $|\Phi_T(x)\rangle = \alpha|1_R,g\rangle - \beta|1_L,e\rangle$. Here we neglect the small phase φ and the spatial dependent phase $\Theta(x)$, which only indicates the opposite propagation directions. We rewrite the state $|\Phi_T(x)\rangle$ as

$$|\Phi_T(x)\rangle = (\alpha|1_R\rangle - \beta|1_L\rangle)|\Psi_+\rangle - (\alpha|1_R\rangle + \beta|1_L\rangle)|\Psi_-\rangle, \tag{38}$$

in the Bell state basis of the flux qubit, where $|\Psi_\pm\rangle = (|e\rangle \pm |g\rangle)/\sqrt{2}$. Clearly, heralded quantum state transfer can be accomplished by measuring the state of the static flux qubit in the Bell basis. A measurement yielding $|\Psi_-\rangle$ projects the flying photonic qubit to $(\alpha|1_R\rangle + \beta|1_L\rangle)$. Here we neglect the trivial global phase of π. The success probability can be 50%. If we obtain $|\Psi_+\rangle$ during the measurement, we need to induce a π phase shift in either path of the photon. In this way, we can do a measurement-based heralded quantum state transfer from the static flux qubit to the flying photonic qubit.

Our scheme can also map the quantum state from the flux qubit to a photonic qubit encoded in the horizontal and vertical polarizations; see Fig. 6. A H-polarized single-photon pulse is injected to the SiV center through an optical circulator. The SiV under the control of the flux qubit scatters this single photon into the right- and left-moving paths. The left-moving part is directed to the lower optical path via the circulator, and then is converted to V polarization by a polarizer. A phase shifter induces a phase θ to the right-moving part in the upper optical path. θ is dependent on the measurement of the flux qubit. When the measurement returns the state $|\Psi_-\rangle$, θ is used to compensate the phase shift induced by the polarizer in the lower optical path, say θ_0. Otherwise, it shifts the phase by $\pi + \theta_0$. Then the two photonic paths are combined by a polarizing beam splitter into the same path, yielding the state $\alpha|H\rangle + \beta|V\rangle$. In doing so, we accomplish the task of a hybrid

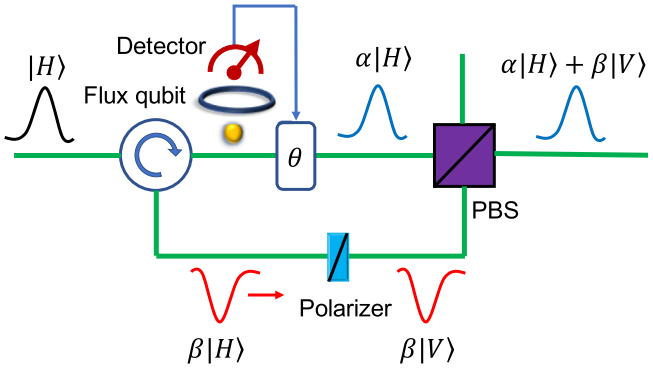

FIG. 6. Schematic diagram for mapping the quantum state from the flux qubit to the photonic qubit.

quantum interface converting quantum information from the microwave regime to the optical. This task is highly desirable towards building a quantum network for superconducting qubits [7–17].

IV. EXPERIMENTAL IMPLEMENTATION

We now estimate the performance of our device for entangling the traveling single photon and the flux qubit, prepared in the superposition state of $(|g\rangle + |e\rangle)/\sqrt{2}$, based on feasible experimental parameters. The decay rate γ_2 of a single SiV is about $2\pi \times 30$ MHz corresponding to a lifetime of ~3 ns [33]. For simplicity, we use $\gamma_1 = \gamma_2$ and $\Gamma = 0$. The applied single-photon pulse has a duration of $\tau_p = 30$ μs. The challenging requirements in the realization of our system are threefold: (i) a large single-spin Zeeman shift; (ii) the long decoherence time of the flux qubit; (iii) a strong coupling between the nanowaveguide and the SiV yielding a Purcell factor larger than 10. This strong coupling has been achieved recently between a single SiV center and a nanowaveguide [43]. Using a flux qubit with a persistent current of 500 nA and a flux concentrator we can achieve a coupling strength of $\eta/2\pi = 300$ kHz. In a recent experiment [63,64], a flux qubit exhibited a longitudinal lifetime of $T_1 \sim 44$ μs and a decoherence time of $T_2 \approx 80$ μs giving a pure dephasing rate $T_2^* \approx 880$ μs [65]. Thus we have $\Gamma^* \approx 2\pi \times 181$ Hz. The energy-relaxation time of the flux qubit is greatly improved by isolating the charge noise with a relative large shunt capacitor, and the flux noise via a capacitive coupling. The flux qubit hardly decays to an open environment since the flux noise from open space is very small at high frequency. In this sense, it is reasonable to assume $T_1 \sim 44$ μs for our flux qubit although the persistent current of our sample is a bit higher than the experimental sample ($I_p = 275$ nA, and $T_1 \sim 40$ μs at ~6 GHz in sample C). The reduction of the relaxation time is mainly due to the shunt capacitor. So, applying a larger shunt capacitor or increasing the separation between the flux qubit and the transmission line can increase the relaxation time T_1. Moreover, the energy relaxation time can be improved by quasiparticle pumping [66]. Since the transmission line is terminated by a SQUID we can further assume that through appropriate tuning we can eliminate the longitudinal relaxation of the flux qubit caused by the flux noise threading in from the terminal line, leading to $\gamma_f = 0$ during the single-photon pulse. This method of isolating a superconducting qubit from its environment has been experimentally proved to be valid [32]. Recent progress in nanowaveguide QED has achieved the strong-coupling regime with a Purcell factor larger than 20 through a variety of methods: using a nanofiber [35], or a dielectric slot nanowaveguide [36], or a photonic crystal waveguide [37–41], or a plasmonic nanowire [42]. We use a Purcell factor of $\Gamma_{wg}/\gamma_2 = 10$ to achieve the strong-coupling regime in our estimates. Using these realistic numbers for parameters in the master equation model, we achieve a high fidelity of $F = 0.87$ and entanglement with a large concurrence of $C = 0.83$. Throughout our numerical investigation, we require $\Omega_c = 0.03\Gamma_{wg} = 2\pi \times 9$ MHz. Considering the large dipole moment of SiV, this classical Rabi frequency can be reached with a weak laser field.

V. DISCUSSION AND CONCLUSION

We have proposed a hybrid quantum interface to route single optical photons into two paths with a flux qubit. Quantum routing of single photons is the key functionality in building a quantum network [3–6], and is useful towards interfacing mw photonics with superconducting quantum circuits [50]. Besides, we have also presented methods to transfer quantum information from the flux qubit to the photonic qubit by first entangling them and then performing a projective measurement. This is another desirable but challenging goal towards building quantum networks for remote quantum communication between solid-state superconducting quantum chips [7–15].

In summary, we have proposed a scheme to conditionally control the routing of a single-photon wave packet by the quantum state of a flux qubit. It is achieved by magnetically tuning the position of an EIT window in a single SiV center interacting strongly with the single photon. Our scheme can create a quantum state of a flying single photon dependent on the quantum state of a flux qubit. The proposed device can act as a hybrid quantum interface and create entanglement between the microwave and optical domains. The atom in the implementation of our device can be, but is not limited to, the SiV defect. It can be some other kind of color centers in a nanodiamond, rare-earth ions in a nanoscrystal, or alkali-metal atoms. We note that a similar scheme has been proposed to entangle two distant superconducting transmon qubits mediated by dipolar molecules strongly coupling to a nanowaveguide [67]. Here we present a relevant scheme for routing single optical photon via a superconducting flux qubit in the quantum regime.

ACKNOWLEDGMENTS

K.X. acknowledges the helpful discussion about the flux qubit with Prof. X. Zhu. This work was partly done in RIKEN in Japan. The work is supported by the National Key R&D Program of China (Grant No. 2017YFA0303703) and the Australian Research Council Centre of Excellence for Engineered Quantum Systems (EQuS), Project No. CE110001013. F.J. also would like to thank the SIQS EC Project No. 600645 and BMBF for support.

[1] H. J. Kimble, Nature (London) **453**, 1023 (2008).
[2] L.-M. Duan and C. Monroe, Rev. Mod. Phys. **82**, 1209 (2010).
[3] C. Chudzicki and F. W. Strauch, Phys. Rev. Lett. **105**, 260501 (2010).
[4] P. J. Pemberton-Ross and A. Kay, Phys. Rev. Lett. **106**, 020503 (2011).
[5] S. Sazim, V. Chiranjeevi, I. Chakrabarty, and K. Srinathan, Quantum Inf. Process. **14**, 4651 (2015).
[6] C. Cao, Y.-W. Duan, X. Chen, R. Zhang, T.-j. Wang, and C. Wang, Opt. Express **25**, 16931 (2017).
[7] Y.-D. Wang and A. A. Clerk, Phys. Rev. Lett. **108**, 153603 (2012).
[8] L. Tian, Phys. Rev. Lett. **108**, 153604 (2012).
[9] S. Barzanjeh, M. Abdi, G. J. Milburn, P. Tombesi, and D. Vitali, Phys. Rev. Lett. **109**, 130503 (2012).
[10] Z. Q. Yin, W. L. Yang, L. Sun, and L. M. Duan, Phys. Rev. A **91**, 012333 (2015).
[11] K. Stannigel, P. Rabl, A. S. Sørensen, P. Zoller, and M. D. Lukin, Phys. Rev. Lett. **105**, 220501 (2010).
[12] K. Xia, M. R. Vanner, and J. Twamley, Sci. Rep. **4**, 5571 (2014).
[13] C. O'Brien, N. Lauk, S. Blum, G. Morigi, and M. Fleischhauer, Phys. Rev. Lett. **113**, 063603 (2014).
[14] L. A. Williamson, Y.-H. Chen, and J. J. Longdell, Phys. Rev. Lett. **113**, 203601 (2014).
[15] K. Xia and J. Twamley, Phys. Rev. A **91**, 042307 (2015).
[16] M. Hafezi, Z. Kim, S. L. Rolston, L. A. Orozco, B. L. Lev, and J. M. Taylor, Phys. Rev. A **85**, 020302(R) (2012).
[17] M. Kiffner, A. Feizpour, K. T. Kaczmarek, D. Jaksch, and J. Nunn, New J. Phys. **18**, 093030 (2016).
[18] X.-Y. Chen, F.-Y. Zhang, and C. Li, J. Opt. Soc. Am. B **33**, 583 (2016).
[19] L. Zhou, L.-P. Yang, Y. Li, and C. P. Sun, Phys. Rev. Lett. **111**, 103604 (2013).
[20] I.-C. Hoi, C. M. Wilson, G. Johansson, T. Palomaki, B. Peropadre, and P. Delsing, Phys. Rev. Lett. **107**, 073601 (2011).
[21] P.-C. Ma, L.-L. Yan, J. Zhang, G.-B. Chen, X.-W. Li, and Y.-B. Zhan, Laser Phys. Lett. **15**, 015204 (2018).
[22] W.-B. Yan and H. Fan, Sci. Rep. **4**, 4820 (2014).
[23] K. Xia and J. Twamley, Phys. Rev. X **3**, 031013 (2013).
[24] K. Xia, G. Lu, G. Lin, Y. Cheng, Y. Niu, S. Gong, and J. Twamley, Phys. Rev. A **90**, 043802 (2014).
[25] T. Aoki, A. S. Parkins, D. J. Alton, C. A. Regal, B. Dayan, E. Ostby, K. J. Vahala, and H. J. Kimble, Phys. Rev. Lett. **102**, 083601 (2009).
[26] I. Shomroni, S. Rosenblum, Y. Lovsky, O. Bechler, G. Guendelman, and B. Dayan, Science **345**, 903 (2014).
[27] X. X. Yuan, J. J. Ma, P.-Y. Hou, X.-Y. Chang, C. Zu, and L.-M. Duan, Sci. Rep. **5**, 12452 (2015).
[28] C. Sayrin, C. Junge, R. Mitsch, B. Albrecht, D. O'Shea, P. Schneeweiss, J. Volz, and A. Rauschenbeutel, Phys. Rev. X **5**, 041036 (2015).
[29] A. Reiserer, N. Kalb, G. Rempe, and S. Ritter, Nature (London) **508**, 237 (2014).
[30] M. Wallquist, V. S. Shumeiko, and G. Wendin, Phys. Rev. B **74**, 224506 (2006).
[31] K. Koshino and Y. Nakamura, New J. Phys. **14**, 043005 (2012).
[32] I. C. Hoi, A. F. Kockum, L. Tornberg, A. Pourkabirian, G. Johansson, and P. Delsing, Nat. Phys. **11**, 1045 (2015).
[33] L. J. Rogers, K. D. Jahnke, M. H. Metsch, A. Sipahigil, J. M. Binder, T. Teraji, H. Sumiya, J. Isoya, M. D. Lukin, P. Hemmer, and F. Jelezko, Phys. Rev. Lett. **113**, 263602 (2014).
[34] B. Pingault, J. N. Becker, C. H. H. Schulte, C. Arend, C. Hepp, T. Godde, A. I. Tartakovskii, M. Markham, C. Becher, and M. Atatüre, Phys. Rev. Lett. **113**, 263601 (2014).
[35] R. Mitch, C. Sayrin, B. Albrecht, P. Schneeweiss, and A. Rauschenbeutel, Nat. Commun. **5**, 5713 (2014).
[36] P. Kolchin, N. Pholchai, M. H. Mikkelsen, J. Oh, S. Ota, M. S. Islam, X. Yin, and X. Zhang, Nano Lett. **15**, 464 (2014).
[37] S. P. Yu, J. D. Hood, J. A. Miniz, M. J. Martin, R. Norte, C. L. Hung, S. M. Meenehan, J. D. Cohen, O. Painter, and H. J. Kimble, Appl. Phys. Lett. **104**, 111103 (2014).
[38] J. S. Douglas, H. Habibian, C. L. Hung, A. V. Gorshkov, H. J. Kimble, and D. E. Chang, Nat. Photonics **9**, 326 (2015).
[39] C. L. Hung, S. M. Meenehan, D. E. Chang, O. Painter, and H. J. Kimble, New J. Phys. **15**, 083026 (2013).
[40] M. Arcari, I. Söllner, A. Javadi, S. Lindskov Hansen, S. Mahmoodian, J. Liu, H. Thyrrestrup, E. H. Lee, J. D. Song, S. Stobbe, and P. Lodahl, Phys. Rev. Lett. **113**, 093603 (2014).
[41] I. Söllner, S. Mahmoodian, S. L. Hansen, L. Midolo, A. Javadi, G. Kiršanskė, T. Pregnolato, H. El-Ella, E. H. Lee, J. D. Song, S. Stobbe, and P. Lodah, Nat. Nanotechnol. **10**, 775 (2015).
[42] D. E. Chang, A. S. Sørensen, E. A. Demler, and M. D. Lukin, Nat. Phys. **3**, 807 (2007).
[43] A. Sipahigil, R. E. Evans, D. D. Sukachev, M. J. Burek, J. Borregaard, M. K. Bhaskar, C. T. Nguyen, J. L. Pacheco, H. A. Atikian, C. Meuwly, R. M. Camacho, F. Jelezko, E. Bielejec, H. Park, M. Lončar, and M. D. Lukin, Science **354**, 847 (2016).
[44] X. Zhu, S. Saito, K. K. A. Kemp, S.-i. Karimoto, H. Nakano, W. J. Munro, Y. Tokura, M. S. Everitt, K. Nemoto, M. Kasu, N. Mizuochi, and K. Semba, Nature (London) **478**, 221 (2011).
[45] K. D. Jahnke, A. Sipahigil, J. M. Binder, M. W. Doherty, M. Metsch, L. J. Rogers, N. B. Manson, M. D. Lukin, and F. Jelezko, New J. Phys. **17**, 043011 (2015).
[46] C. M. Wilson, G. Johansson, A. Pourkabirian, M. Simoen, J. R. Johansson, T. Duty, F. Nori, and P. Delsing, Nature (London) **479**, 376 (2011).
[47] T. P. Orlando, J. F. Mooij, L. Tian, C. H. van der Wal, L. S. Levitov, S. Lloyd, and J. J. Mazo, Phys. Rev. B **60**, 15398 (1999).
[48] O. Astafiev, A. M. Zagoskin, A. A. Abdumalikov, Y. Pashkin, T. Yamamoto, K. Inomata, Y. Nakamura, and J. S. Tsai, Science **327**, 840 (2010).
[49] K. Xia, M. Macovei, and J. Evers, Phys. Rev. B **84**, 184510 (2011).
[50] X. Gu, A. F. Kockum, A. Miranowicz, Y.-X. Liu, and F. Nori, Phys. Rep. **718-719**, 1 (2017).
[51] J.-T. Shen and S. Fan, Phys. Rev. A **79**, 023837 (2009).
[52] J.-T. Shen and S. Fan, Phys. Rev. A **79**, 023838 (2009).
[53] C. W. Gardiner, Phys. Rev. Lett. **70**, 2269 (1993).
[54] H. J. Carmichael, Phys. Rev. Lett. **70**, 2273 (1993).
[55] W. K. Wootters, Phys. Rev. Lett. **80**, 2245 (1998).
[56] Y. Tabuchi, S. Ishino, A. Noguchi, T. Ishikawa, R. Yamazaki, K. Usami, and Y. Nakamura, Science **349**, 405 (2015).
[57] C. Navau, J. Prat-Camps, O. Romero-Isart, J. I. Cirac, and A. Sanchez, Phys. Rev. Lett. **112**, 253901 (2014).
[58] W. C. Griffith, R. Jimenez-Martinez, V. Shah, S. Knappe, and J. Kitching, Appl. Phys. Lett. **94**, 023502 (2009).

[59] C. Tsang, C. Bonhote, Q. Dai, H. Do, B. Knigge, Y. Ikeda, Q. Le, B. Lengsfield, J. Lille, J. Li, S. MacDonald, A. Moser, V. Nayak, R. Payne, N. Robertson, M. Schabes, N. Smith, K. Takano, P. van der Heijden, W. Weresin, M. Williams, and M. Xiao, IEEE Trans. Magn. **42**, 145 (2006).

[60] L. Trifunovic, F. L. Pedrocchi, S. Hoffman, P. Maletinsky, A. Yacoby, and D. Loss, Nat. Nanotechnol. **10**, 541 (2015).

[61] T. Douce, M. Stern, N. Zagury, P. Bertet, and P. Milman, Phys. Rev. A **92**, 052335 (2015).

[62] G. Cordourier-Maruri, F. Ciccarello, Y. Omar, M. Zarcone, R. de Coss, and S. Bose, Phys. Rev. A **82**, 052313 (2010).

[63] F. Yan, S. Gustavsson, A. Kamal, J. Birenbaum, A. Sears, D. Hover, T. J. Gudmundsen, J. L. Yoder, T. P. Orlando, J. Clarke, A. Kerman, and W. D. Oliver, Nat. Commun. **7**, 12964 (2016).

[64] M. Stern, G. Catelani, Y. Kubo, C. Grezes, A. Bienfait, D. Vion, D. Esteve, and P. Bertet, Phys. Rev. Lett. **113**, 123601 (2014).

[65] J. Clarke and F. K. Wilhelm, Nature (London) **453**, 1031 (2008).

[66] S. Gustavsson, F. Yan, G. Catelani, J. Bylander, A. Kamal, J. Birenbaum, D. Hover, D. Rosenberg, G. Samach, A. P. Sears, S. J. Weber, J. L. Yoder, J. Clarke, A. J. Kerman, F. Yoshihara, Y. Nakamura, T. P. Orlando, and W. D. Oliver, Science **354**, 1573 (2016).

[67] S. Das, V. E. Elfving, S. Faez, and A. S. Sørensen, Phys. Rev. Lett. **118**, 140501 (2017).